perimentally testable with modern synthetic peptide techniques.[17] If many pathways are important, the rate should be weakly dependent on the details of the intervening medium.

Finally, we emphasize that this theoretical work is of a survey nature aimed at providing design and interpretation guidelines. Interpretation of transfer rates requires corrections due to differences in reaction free energies, reorganization energies, and tunneling matrix element prefactors (donor–first bridge orbital and last bridge orbital–acceptor coupling factors) prior to attempting a correlation with pathway length. From a theoretical point of view, interference between multiple pathways, high-order (multiple scattering) corrections, bond orientation, and energetic effects have been neglected. The importance of these effects in causing qualitative changes in the pathways and quantitative changes in the couplings is being investigated. In spite of the limitations of the calculations, this work describes the physical mechanism for electron tunneling through the protein environment and it provides a tool to guide the design and interpretation of new protein-electron-transfer experiments. Preliminary results from this study, especially on cytochrome *c*, are encouraging since effective tunneling pathway lengths correlate very well with experimental estimates of the tunneling matrix elements.[14]

VI. Software

Software was developed with the Digital Equipment implementation of FORTRAN 77 to run on Digital Vax and Microvax machines. The source code and users manual are available from the authors.[18] The program inputs parameters from four data files and one BIOGRAF[19] structure file derived from the X-ray crystal structure. The software outputs an ascii file listing the pathways and a BIOGRAF vector file with their coordinates.

Acknowledgment. This work was performed in part at the Jet Propulsion Laboratory, California Institute of Technology and was sponsored in part by the Department of Energy's Energy Conversion and Utilization Technologies Division—ECUT, through an agreement with the National Aeronautics and Space Administration. Particular credit is due Minoo Dastoor, whose support and encouragement made this work possible. J.B. thanks Caltech for a Summer Undergraduate Research Fellowship (SURF). B.B. acknowledges the Medical Research Council (Canada) for a postdoctoral fellowship. J.N.O. and D.N.B. thank the National Science Foundation and CNPq (Brazil) for a Binational Research Grant that allowed international visits during which much of this work was performed and the Brazilian agencies FINEP and CNPq for additional support. J.N.O. also thanks the University of California, San Diego for start-up funding support. Work on protein electron transfer at Caltech (H.B.G.) is supported by grants from the National Science Foundation and the National Institutes of Health.

(17) Raphael, A. L.; Gray, H. B. *Proteins* **1989**, *6*, 338.

(18) A users guide to the pathway program, written by B. E. Bowler, J. Betts, and D. N. Beratan, 1989. The software has recently been modified to run on Silicon graphics workstations.

(19) BIOGRAF is a product of Biodesign, Inc., Pasadena, CA.

Analysis of Intramolecular Motions by Filtering Molecular Dynamics Trajectories

Pnina Dauber-Osguthorpe and David J. Osguthorpe*

Contribution from the Molecular Graphics Unit, University of Bath, Claverton Down, Bath BA2 7AY, UK. *Received December 20, 1989*

Abstract: A novel method for analyzing molecular dynamics trajectories has been developed, which uses digital signal processing techniques to eliminate unwanted motion and retains only motions of interest. In particular, it is possible to filter out the high-frequency motions and focus on the low-frequency collective motions of molecules. The trajectories of each of the atoms in the system (or any subset of interest) are Fourier transformed to the frequency domain, a filtering function is applied, and then an inverse transformation back to the time domain yields the filtered trajectory. The validity and merits of the filtering method were studied in detail for acetamide and *N*-acetylalanine-*N'*-methylamide as models for peptides and proteins. Initially the technique was tested for fluctuations around one local minimum. The normal modes obtained by diagonalizing the mass-weighted second-derivative matrix were combined to generate a well-characterized "normal-mode trajectory". The frequency distribution of this trajectory approximates a δ function with a peak for each of the frequencies in the normal-mode analysis. By use of a filtering function that retains only one peak of the spectral distribution, a single mode was extracted. This filtered mode had all the characteristics of the original normal mode. Technical aspects such as the effects of simulation length and sampling frequency were also examined by using normal-mode trajectories. The method was then applied to "real" molecular dynamics trajectories. We have shown that information about the structural mobility at the vicinity of a minimum, traditionally obtained from normal-mode analysis, can also be extracted from molecular dynamics simulations by using the filtering technique. In addition, molecular dynamics simulations that include conformational transitions, such as $\alpha_R \rightarrow C_7^{eq}$, were used for evaluating the merits of the filtering technique in anharmonic regions. We concluded that with this technique it is possible to characterize the important motions of a molecule in a way analogous to normal-mode analysis, without confining the study to harmonic oscillations and one local minimum energy conformation. The filtering technique is very flexible and can easily be applied to sections of a molecule or whole molecular systems, and various types of motion can be selected by designing the appropriate filtering function. Since it is also not very demanding computationally, it can serve as a powerful tool for the characterization of the dynamic behavior of small and large molecular systems.

Introduction

Molecular mechanics calculations have been used since the late 1960s[1,2] as an important tool for understanding the structural and energetic preferences of molecules.[3,4] In recent years the theoretical (and experimental) study of the dynamic behavior of molecules expanded as well. In particular, the flexibility and internal motion of biomolecules such as proteins (enzymes, receptors, etc.) or nucleic acids (DNA and RNA) are of importance

(1) Lifson, S.; Warshel, A. *J. Chem. Phys.* **1968**, *49*, 5116.
(2) Allinger, N. L.; Sprague, J. T. *J. Am. Chem. Soc.* **1972**, *94*, 5734.
(3) Ermer, O. *Struct. Bonding (Berlin)* **1976**, *27*, 161.

(4) Burkert, U.; Allinger, N. L. In *Molecular Mechanics*; ACS Monograph Series 177; American Chemical Society, Washington, Dc, 1982.

0002-7863/90/1512-7921$02.50/0

in biological events. Phenomena such as domain closure on ligand binding,[5] allosteric effects,[6] and partial DNA helix unwinding during intercalating drug binding[7,8] involve collective motion of large parts of the molecules. Investigation of such delocalized slow motions is thus of great interest. Molecular dynamics simulations have been applied to many molecular systems, from small peptides[9-12] to large assemblies of molecules such as protein–ligand systems.[13] Some of the recent applications used molecular dynamics only as a means for exploring conformational space or refining structure in combination with X-ray or NMR data.[14] Other studies used the trajectories to obtain average properties and compare those to experimental values (for a review, see ref 15). The exploration of the nature of the motion itself has not yet been a common practice.

In order to gain insight into the dynamic behavior of molecules (or molecular systems) it is important to be able to identify different types of motion and characterize them. One approach to this problem has long been used in the interpretation of vibrational spectra, namely, normal-mode analysis (see for example refs 16 and 17 for hydrocarbons). This analysis provides a set of characteristic frequencies and the corresponding motions (normal modes).[18,19] The merits of this method are that it provides a "pictorial" description of the various modes of motion and enables a selective study of the motions of interest as well as the ability to calculate thermodynamic properties. However, this method assumes small harmonic motion in the vicinity of one local minimum. Thus, it is not applicable for the study of motions involving large anharmonic fluctuations or conformational transitions. In addition, the requirements for a fully minimized structure and diagonalization of a second-derivative matrix result in a large computational problem, which led to the introduction of further approximations (e.g., nonconvergent minimizations and rigid geometry) in applications to large systems.[20-22] The molecular dynamics simulation, on the other hand, results in a trajectory that represents a realistic and comprehensive description of molecular motion. It takes into account full flexibility of the molecules, including conformational transitions, and is applicable to harmonic and anharmonic regions of the potential surface. Although the laws governing the molecular dynamics, i.e., Newton's equations of motion, are simple, the combined effect of the many forces exerted on each atom can yield a trajectory that appears quite complicated and in many cases resembles "random noise". Interpreting such complex motion is thus a very difficult and interesting problem, which we address in this study.

We have developed a methodology that utilizes the frequency distribution as a tool for partitioning the overall motion into characteristic motions, and a novel filtering technique that enables us then to focus on those motions which are of interest or importance. The characterization is achieved by Fourier transforming the trajectories of Cartesian or internal coordinates to yield the frequency distribution. Subsequently, we can choose the frequencies corresponding to the motion of interest and by applying digital signal techniques filter out the unwanted frequency ranges. Of particular interest is the ability to remove the high-frequency bond stretches and valence angle bending and to focus on the low-frequency conformational motions.

The filtering technique was applied to the enzyme phospholipase A_2 to demonstrate its merits in the analysis of motion in a biological system and revealed interesting delocalized motions such as "concertina" movement of helices and changes in shape and size of the active-site cavity.[23] In this paper we describe the method and test its merits on small molecules. First we studied the motions at the vicinity of a local minimum by creating a "normal-mode trajectory", in which the motions are well defined, and tested the ability of the filtering method to extract the underlying components of motion. The effects of applying this method to a "real" molecular dynamics trajectory of the same molecule were examined next and compared to the dynamic behavior obtained from the normal-mode trajectory. Motions in anharmonic regions of the potential surface, including conformational transitions, were studied next. We concentrate in this paper on the characterization of structural properties at local minima and during conformational transitions. Applying the filtering technique to the understanding of the associated energetics of conformational fluctuations and transitions will be discussed elsewhere.[24]

Methods

Energy Function. The calculations performed in this study are all based on a representation of the molecules as fully flexible. The potential energy of the system is represented by an analytical function of internal coordinates (including bonds, valence angles, torsion angles, out of plane angles, and cross terms) and interatomic distances. The parameters for this function were refined to reproduce experimental data of a set of model compounds including functional groups that occur in amino acids.[25-27]

Minimization. Minimization prior to molecular dynamics is required in order to alleviate strain in the initial structure, which could lead to generation of "hot spots" and thus spurious motions during the molecular dynamics simulations. Fully minimized structures are required for normal-mode analysis since this method is based on the assumption that small fluctuations around a *minimum energy* structure are occurring. A quasi Newton algorithm was employed to minimize the energy.[28]

Generation of Trajectories. The motion of an assembly of particles is described in classical mechanics by the Lagrange equations of motion:

$$\frac{d}{dt}\frac{\partial K}{\partial \dot{q}_i} + \frac{\partial V}{\partial q_i} = 0 \quad i = 1, 2, 3, ..., 3n \tag{1}$$

where K and V are the kinetic and potential energy of the system, and q and $\dot{q}$ are the coordinate and velocity, respectively. In a system of Cartesian coordinates, x_i (and corresponding velocities and accelerations, $\dot{x}_i$ and $\ddot{x}_i$, respectively), this corresponds to Newton's equations of motion:

$$F_i = m_i\ddot{x}_i = -\frac{\partial V}{\partial x_i} \quad i = 1, 2, 3, ..., 3n \tag{2}$$

(a) Molecular Dynamics Trajectories. In molecular dynamics simulations, Newton's equations of motion (eq 2) are solved numerically.[13,29]

(5) Remington, S.; Wiegand, G.; Huber, R. *J. Mol. Biol.* **1982**, *158*, 111–152.
(6) Fletterick, R. J.; Madsen, N. B. *Trends Biochem. Sci.* **1977**, 145–148.
(7) *Antibiotics, Mechanism of Action of Antieukaryotic and Antiviral Comounds*; Springer-Verlag: Berlin, 1979; Vol. 2, pp 195–213.
(8) Neidle, S.; Waring, M. J. *Molecular Aspects of Anti-Cancer Drug Action*; Macmillan Press: London 1983.
(9) Hagler, A. T.; Osguthorpe, D. J.; Dauber-Osguthorpe, P.; Hempel, J. C. *Science* **1985**, *227*, 1309–1315.
(10) Hassan, M.; Goodman, M. *Biochemistry* **1986**, *25*, 7596–7606.
(11) Brown, D. W.; Campbell, M. M.; Kinsman, R. G.; Moss, C.; Paul, P. K. C.; Osguthorpe, D. J.; Baker, B. *J. Chem., Soc. Chem. Commun.* **1988**, 1543–1545.
(12) Paul, P. K. C.; Dauber-Osguthorpe, P.; Campbell, M. M.; Brown, D. W.; Kinsman, R. G.; Moss, C.; Osguthorpe, D. J. *Biopolymers* **1990**, *29*, 623–637.
(13) McCammon, J. A.; Harvey, S. C. *Dynamics of Proteins and Nucleic Acids*; Cambridge University Press: Cambridge, England, 1987.
(14) Karplus, M.; Brunger, A. T.; Elber, R.; Kuriyan, J. *Cold Spring Harbor Symp. Quant. Biol.* **1987**, *52*, 381–390.
(15) Levy, R. M.; Keepers, J. W. *Comments Mol. Cell. Biophys.* **1984**, *3*, 273–294.
(16) Snyder, R. G.; Schachtschneider, J. H. *Spectrochim. Acta* **1963**, *19*, 85–116.
(17) Califano, S. *Pure Appl. Chem.* **1969**, *18*, 353.
(18) Wilson, E. B.; Decius, J. C.; Cross, P. C. *Molecular Vibrations*; McGraw Hill: New York, 1955.
(19) Herzberg, G. *Molecular Spectra and Molecular Structure II. Infrared and Raman Spectra of Polyatomic Molecules*; D. van Nostrand Co.: New York, 1945.
(20) Levitt, M.; Sander, C.; Stern, P. S. *J. Mol. Biol.* **1985**, *181*, 423–447.
(21) Brooks, B.; Karplus, M. *Proc. Natl. Acad. Sci. U.S.A.* **1985**, *82*, 4995–4999.
(22) Nishikawa, T.; Go, N. *Proteins: Struct., Funct., Genet.* **1987**, *2*, 308–329.
(23) Sessions, R. B.; Dauber-Osguthorpe, P.; Osguthorpe, D. J. *J. Mol. Biol* **1989**, *210*, 617–634.
(24) Dauber-Osguthorpe, P.; Osguthorpe, D. J. *Biochemistry*, in press.
(25) Dauber-Osguthorpe, P.; Roberts, V. A.; Osguthorpe, D. J.; Wolff, J.; Genest, M.; Hagler, A. T. *Proteins: Struct., Funct., Genet.* **1988**, *4*, 31–47.
(26) Hagler, A. T.; Huler, E.; Lifson, S. *J. Am. Chem. Soc.* **1974**, *96*, 5319–5326.
(27) Lifson, S.; Hagler, A. T.; Dauber, P. *J. Am. Chem. Soc.* **1979**, *101*, 5111–5121.
(28) Fletcher, R. *Practical Methods of Optimization*; Wiley: New York, 1980; Vol. 1.

The forces on each atom and, hence, the acceleration, are calculated from the gradient of the potential energy, and a small time step ($\Delta t \approx 10^{-15}$ s) is applied to generate the next set of coordinates and velocities. We carried out the integration using Verlet's second-order algorithm.[30]

(b) Normal-Mode Trajectories. Another approach to the solution of the Lagrange equation was taken in normal-mode analysis.[18,19] Only small fluctuations around a minimum-energy conformation are considered and the potential energy is approximated by a harmonic (multidimensional quadratic) function of the coordinates. In this approximation, the solution of the Lagrange eq 1 involves diagonalizing the matrix of second derivatives of the energy with respect to the coordinates. In a coordinate system of mass-weighted Cartesian displacements, $q_i = m_i^{1/2}(x_i - x_i^0)$, a set of $3n$ solutions is obtained:

$$q_i = l_{ik} \cos(\nu_k t + \epsilon_k) \quad k = 1, 2, 3, ..., 3n \tag{3}$$

where the ν_k, ϵ_k, and l_{ik} are the set of characteristic frequencies, phases, and normal modes of motion, respectively. The general solution to the equations of motion, which defines the total motion and potential energy of the system is given by

$$q_i = \sum_{k=1}^{3n-6} l_{ik} A_k \cos(\nu_k t + E_k) \tag{4}$$

$$V = \tfrac{1}{2} \sum_{k=1}^{3n-6} \nu_k^2 A_k \cos^2(\nu_k t + \epsilon_k)$$

where A_k define the maximum amplitudes, which are determined by the temperature in the system. We used normal-mode trajectories as a first test case for the filtering method (see below). These trajectories represent well-defined regular motion and thus the expected result from filtering is known a priori.

Analysis of Trajectories. The analysis of the trajectories was carried out with the software package FOCUS.[31] This package uses the trajectories of atomic positions and velocities and energies to calculate (and plot) trajectories of related properties such as internal coordinates, interatomic distances, etc. and statistical averages and standard deviations. The program also calculates frequency distributions (and thermodynamic properties) and filters out selective types of motion as described below.

(a) Frequency Distribution. The frequency distribution function, $g(\nu)$, gives the number of characteristic motions in the system with a frequency ν. This function has been obtained from the trajectories of atomic velocities[32] and can be obtained from the trajectories of atomic coordinates as well. The frequency distribution can be derived from the distribution of kinetic energy as a function of frequency:

$$\sum_{k=1}^{N} K(\nu_k) = \langle K \rangle = \frac{1}{2N} \sum_{i=1}^{n} \sum_{l=1}^{N} \dot{q}_i^2(t_l) = \frac{1}{2N^2} \sum_{i=1}^{n} \sum_{k=1}^{N} |\dot{Q}_i(\nu_k)|^2 = \frac{1}{2N^2} \sum_{k=1}^{N} \dot{F}_i(\nu_k) \tag{5}$$

where q_i and $\dot{q}_i$ are the mass-weighted coordinates and velocities, Q_i and $\dot{Q}_i$ are the corresponding Fourier transforms (FT), and N is the number of time steps in the trajectory. Parseval's theorem was used in replacing the summation in time domain with summation in the frequency domain.[33] Thus

$$K(\nu_k) = \frac{1}{2N^2} \dot{F}(\nu_k) \tag{6}$$

Since the kinetic energy is harmonic, the equipartition of energy implies that each degree of freedom has $\frac{1}{2}\mathbf{k}T$ in energy, or $\frac{1}{2}(3n-6)\mathbf{k}T$ in total (assuming no global rotation and translation). Since the integral of the frequency distribution is $3n - 6$, $g(\nu)$ is given by

$$g(\nu_k) = \frac{1}{N^2 \mathbf{k} T} \dot{F}(\nu_k) \tag{7}$$

For a harmonic potential, the frequency distribution in terms of coordinate trajectories can be obtained in an analogous way. However, it can be shown that the frequency distribution can be obtained from the trajectories of the coordinates, for any form of potential (assuming only that the discrete FT of the velocity trajectory is a good representation of the continuous FT). Using the equations defining the FT pair for a general function,[33] we can get the velocity FT pair and, by integration with respect to time, the coordinate FT pair:

$$\dot{q}(t_l) = \sum_{k=1}^{N} [A_k \cos(\nu_k t_l) + B_k \sin(\nu_k t_l)] \quad \dot{Q}(\nu_k) = \tfrac{1}{2}A_k + j\tfrac{1}{2}B_k \tag{8}$$

$$q(t_l) = \sum_{k=1}^{N} [A_k \nu_k \sin(\nu_k t_l) - B_k \nu_l \cos(\nu_k t_l)] \quad Q(\nu_k) = -\tfrac{1}{2}\nu_k B_k + j\tfrac{1}{2}\nu_k A_k$$

Thus

$$|\dot{Q}(\nu_k)|^2 = \nu_k^2 |Q(\nu_k)|^2 \tag{9}$$

Substituting eq 9 in eqs 6 and 7, we get the frequency and kinetic energy distribution in terms of coordinates:

$$K(\nu_k) = \frac{\nu_k^2}{N^2} F(\nu_k) \tag{10}$$

$$g(\nu_k) = \frac{\nu_k^2}{N^2 \mathbf{k} T} F(\nu_k) \tag{11}$$

where

$$F(\nu_k) = \sum_{i=1}^{n} |Q_i(\nu_k)|^2$$

The thermodynamic properties such as entropy and free energy can be obtained from $g(\nu)$ by use of the Einstein equations.[34]

(b) Filtering Molecular Dynamics Trajectories. The filtering method we developed is based on digital signal processing techniques, in which filtering is used to remove "noise" from an electronic signal.[35,36] Here the individual atomic trajectories are treated in an analogous way to electronic signals. The technique involves three steps: (a) Fourier transforming each atomic trajectory to the frequency domain, (b) applying a filtering function to remove the unwanted frequency components, (c) inverse Fourier transforming back to the time domain. By use of the discrete FT definitions[33]

$$X_i(\nu_k) = 1/N \sum_{l=1}^{N} x_i(t_l) e^{-j\nu_k t_l / N} \tag{12a}$$

$$F(\nu_k) = 1 \quad \nu_{min} < \nu_k < \nu_{max} \tag{12b}$$

$$F(\nu_k) = 0 \quad \nu_k < \nu_{min};\ \nu_k > \nu_{max}$$

$$X_i'(\nu_k) = X_i(\nu_k) F(\nu_k)$$

$$x_i'(t_l) = \sum_{l=1}^{N} X_i'(\nu_k) e^{j\nu_k t_l / N} \tag{12c}$$

The range of frequencies maintained by the filtering function, ν_{min} to ν_{max}, is termed the "band pass". A "low-pass" filter is defined by $\nu_{min} = 0$ and removes all frequencies above a finite ν_{max}, while a "high-pass" filter is defined by $\nu_{max} = \infty$ and removes all frequencies below $\nu_{min} \neq 0$.

Any other structural property, such as interatomic distance, bond length, valence angle, or torsion angle can be treated in an analogous way. The same method can be applied also to filtering energy properties.[24] However, the frequencies of oscillation of the potential energy are double the frequencies of the internals. Since both positive and negative deviations of the coordinates from their equilibrium yield a positive energy, two cycles of the potential energy are completed for each cycle of a coordinate oscillation.

Results and Discussion

Simulations of Model Compounds. The filtering method has been applied to acetamide (schematic I) and a blocked alanine, *N*-acetylalanine-*N'*-methylamide (schematic II). The energies of the two molecules were minimized and then a normal-mode calculation was carried out. The calculated and observed[37-39] frequencies and their assignment for acetamide are given in Table

(29) Allen, M. P.; Tildesley, D. J. *Computer Simulation of Liquids*; Clarendon: Oxford, England, 1987.
(30) Verlet, L. *Phys. Rev.* **1967**, *159*, 98.
(31) Dauber-Osguthorpe, P.; Sessions, R. B.; Osguthorpe, D. J. *FOCUS, (Finally One Can Understand Simulations)*, version 1.0; Molecular Modelling Unit, University of Bath: Bath, UK, 1988.
(32) Berens, P. H.; Mackay, D. H. J. White, G. M.; Wilson, K. R. *J. Chem. Phys.* **1983**, *79*, 2375-2389.
(33) Brigham, E. O. *The Fast Fourier Transform and its Applications*; Prentice-Hall: Englewood Cliffs, NJ, 1988.
(34) Hill, T. L. *An Introduction to Statistical Thermodynamics*; Addison-Wesley: Reading, MA, 1960.
(35) Oppenheim, A. V.; Schafer, R. W. *Digital Signal Processing*; Prentice-Hall International: London, 1975.
(36) A conceptually similar approach was used in early determinations of normal vibrations by building mechanical models of the vibrating molecules and using stroboscopes to identify particular frequencies. (See ref 19, p 157.)
(37) King, S. T. *Spectrochim. Acta* **1972**, *28A*, 165-175.
(38) Kutselnigg, W.; Mecke, R. *Spectrochim. Acta* **1962**, *18*, 549-560.
(39) Kydd, R. A.; Dunham, A. R. C. *J. Mol. Struct.* **1980**, *69*, 79-88.

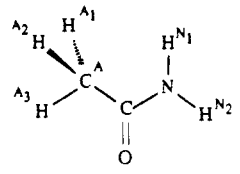

I

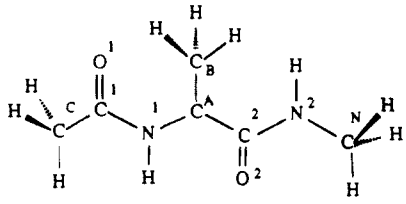

II

I. The assignments were made according to the calculated normal modes. The minimized (and experimental[40]) structure of acetamide is given in Table II, and the minimized structures of two conformations of the blocked alanine, C_7^{eq} and α_R, are given in Table IV.

The first stage of testing the method involved a normal-mode trajectory for acetamide. The normal-mode trajectory was generated by using eqs 4 with all normal modes included, and the A_k were chosen so that each normal mode oscillates with the same energy. The frequency distribution function, $g(\nu)$, was calculated by using eq 11. The effects of the simulation length and the sampling frequency on the frequency distribution were examined first in order to establish suitable conditions for filtering. The results of applying a low- and a high-pass filter on the normal-mode trajectory were examined next. Equation 12 was used with ν_{max} = 170 cm^{-1}, for the low-pass filter and ν_{min} = 3200 cm^{-1}, for the high-pass filter. These filtered trajectories were compared to normal-mode trajectories generated by using only mode 21, and by using a superposition of only modes 1 and 2 (see Table I).

The following step involved "real" molecular dynamics trajectories. A trajectory of ≈132 ps was generated for acetamide. In order to ensure that all possible motions of the molecule are active in the simulation, the initial structure was generated by superimposing on the minimum-energy structure distortions along all normal modes, with amplitudes consistent with equal energy for each mode. Due to the anharmonic nature of real distortions, amplitudes consistent with 150 K had to be used to avoid nonbond clashes. The initial velocities were set to 0 so that the initial motion was determined solely by the distortions in structure. After the excess potential energy was redistributed, an average temperature of ≈300 K was reached. No temperature rescaling was necessary since the total energy was conserved throughout the simulation.

In order to investigate some fundamental motions of peptides and proteins, a molecular dynamics simulation of the model dipeptide *N*-acetylalanine-*N'*-methylamide was carried out. This simulation was started from a structure with $(\phi, \psi) \approx -80, 0$ (which is not a local minimum), in order to induce conformational transitions. It was carried out for 133 ps, and the resultant trajectory included a number of conformational transitions between the C_7^{eq} conformation $(\phi, \psi) = -80, 80$, and the helical α_R conformation $(\phi, \psi) = -80, -40$. The blocking methyl groups rotate nearly freely, whereas χ and the amide bond torsions, ω, fluctuate around one equilibrium value.

Effect of Simulation Length and Sampling Frequency. The ability of the discrete FT to approximate a continuous FT was tested on a normal-mode trajectory of acetamide. In particular the effects of time domain truncation and sampling are examined in some detail in order to elucidate the conditions for successful application of the FT and filtering methods. The dependence of $g(\nu)$ on the total duration and on the frequency of sampling of the time domain function are shown in Figures 1 and 2, respectively.

Table I. Vibrational Frequencies of Acetamide

no.	frequency[a] calcd	frequency[a] obsd[b]	assignment[c]
1	3582	3557	(a′) a-ν(NH_2)
2	3469	3436	(a′) s-ν(NH_2)
3	2990	2967	(a″) ν(CH_3)
4	2987	2900	(a′) a-ν(CH_3)
5	2885	2860	(a′) s-ν(CH_3)
6	1684	1728	(a′) ν(C=O)
7	1589	1589	(a′) δ(NH_2)
8	1459	1432	(a′) a-δ(CH_3)
9	1444	1432	(a″) δ(CH_3)
10	1363	1370	(a′) s-δ(CH_3)
11	1338	1316	(a′) ν(CN,CC), δ(CNH,OCN)
12	1052	1134	(a″) ρ(CH_3)
13	1006	1038	(a′) ρ(CH_3)
14	965	970	(a′) ρ(NH_2)
15	814	840	(a′) ν(CC,CN)
16	551	622	(a″) τ(NH_2), ω(CO), ω(NH_2)
17	507	547	(a′) δ(OCN,CCO)
18	434	427	(a′) δ(CCN,CCO,OCN)
19	423	508	(a″) τ(NH_2)
20	245	268	(a″) ω(NH_2), τ(NH_2)
21	93		(a″) τ(CH_3)

[a] Frequencies are in reciprocal centimeters. [b] Most observed frequencies are from Ar matrix spectra.[37] Vibrations 3–5 and 12 are from gas-phase measurements.[38] (In general the agreement between the observed frequencies in Ar and in vapor is within 5 cm^{-1}). [c] ν is a stretching mode; δ is a deformation (bend) mode; τ is a torsion mode; ρ is a rocking mode; ω is a wagging (out of plane) mode.

Figure 1a–d shows the frequency distributions for simulations of decreasing duration starting at 64 ps and going down to 0.5 ps. In general, the frequency distribution resembles a set of δ functions with "peaks" at frequencies corresponding to the characteristic frequencies obtained from the normal-mode analysis (see Table I). In particular, in (a) the height of most peaks is close to 1, i.e., each peak corresponds to one normal mode. In fact, the integral of $g(\nu)$ indicates that even lower peaks correspond to one frequency, with a total of 21 ($3n - 6$) frequencies. The broadening of the bands for shorter simulations is due to the truncation of the periodic time domain function. Two factors contribute to the width of the bands. First, the resolution in frequency domain is defined by $1/t^{tot}$, where t^{tot} is the length of the simulation. In addition, truncation of the time domain wave function at a time other than a multiple of the period introduces additional frequency components in the frequency domain function. This effect, called leakage, is worse the smaller the number of periods that were included in the time function. Thus, for the shorter trajectories the leakage is more noticeable, and low-frequency waves are more affected then the higher frequencies. For example, in Figure 1d there is a significant "base line", which is due, almost solely, to the leakage of the lowest frequency mode. To demonstrate this point, the frequency distributions of 0.5-ps trajectories of normal mode 21 only and of normal modes 1–20 are shown in Figure 1e and f, respectively. It can clearly be seen that normal mode 21 is responsible for most of the leakage into the "base line".

The other aspect of discrete FT that may distort the results is the frequency of sampling in the time domain. In order to obtain all the frequency components of the time function, the rate of sampling must be at least twice the highest frequency component in the wave. ($\nu_{max} = {}^1/_2\, dt$). Sampling every 4 ps corresponds to a maximum frequency of 4170 cm^{-1}. Since the vibrational frequencies of molecules are lower than 4000 cm^{-1}, more frequent sampling of the trajectory is not necessary. In Figure 2 the frequency distribution of a normal-mode trajectory of acetamide is shown for sampling frequencies from 5 to 10 ps. Figure 1a, which was obtained by sampling every 4 ps, represents a full spectrum of the molecule. However, in Figure 2a, sampling every

(40) Kimura, M.; Aoki, M. *Bull. Chem. Soc. Jpn.* **1953**, *26*, 429–433.

Table II. Geometry and Mobility of Acetamide (Normal-Modes Trajectory)[a]

		all modes		filtered (0–170)[b]		mode 21		filtered (>3200)[b]		modes 1 and 2	
internal	minimized[c]	⟨P⟩	σ	⟨P⟩	σ	⟨P⟩	σ	⟨P⟩	σ	⟨P⟩	σ
bonds											
CA-HA1	1.104	1.213	0.081	1.209	0.073	1.209	0.073	1.104	0.000	1.104	0.000
CA-HA2	1.104	1.213	0.081	1.209	0.071	1.209	0.073	1.104	0.000	1.104	0.000
CA-HA3	1.104	1.209	0.078	1.205	0.070	1.205	0.070	1.104	0.000	1.104	0.000
CA-C	1.502	1.503	0.031	1.502	0.001	1.502	0.000	1.502	0.000	1.502	0.000
C-O	1.223	1.226	0.022	1.225	0.001	1.225	0.001	1.223	0.000	1.223	0.000
C-N	1.306	1.308	0.027	1.307	0.000	1.307	0.001	1.306	0.001	1.306	0.001
N-HN1	1.022	1.069	0.047	1.022	0.000	1.022	0.000	1.022	0.024	1.022	0.024
N-HN2	1.023	1.060	0.043	1.023	0.000	1.023	0.000	1.023	0.024	1.023	0.025
angles											
HA1-CA-HA2	108.4	109.9	4.19	110.0	1.10	110.0	1.10	108.3	0.03	108.4	0.02
HA1-CA-HA3	107.1	108.9	4.24	109.0	1.29	109.0	1.29	107.1	0.02	107.1	0.02
HA1-CA-C	111.8	109.9	4.11	109.9	1.67	109.9	1.67	111.8	0.03	111.8	0.03
HA2-CA-HA3	107.1	108.9	4.27	109.0	1.29	109.0	1.28	107.1	0.01	107.1	0.01
HA2-CA-C	111.8	109.9	4.11	109.9	1.67	109.9	1.67	111.8	0.01	111.8	0.03
HA3-CA-C	110.6	108.8	3.94	108.8	1.20	108.8	1.19	110.6	0.02	110.6	0.03
CA-C-O	122.5	122.3	3.12	122.5	0.02	122.5	0.04	122.5	0.02	122.5	0.02
CA-C-N	117.3	117.2	3.17	117.3	0.03	117.3	0.02	117.3	0.09	117.3	0.10
O-C-N	120.1	120.0	3.17	120.2	0.03	120.2	0.03	120.1	0.09	120.1	0.10
C-N-HN1	116.9	115.5	4.37	116.9	0.02	116.9	0.02	116.9	0.16	116.9	0.16
C-N-HN2	114.2	113.2	4.36	114.2	0.04	114.2	0.04	114.2	0.17	114.2	0.16
HN1-N-HN2	128.9	123.3	5.78	128.9	0.04	128.9	0.03	128.9	0.13	128.9	0.14
torsions											
HA1-CA-C-O	119.2	119.4	28.40	119.4	28.10	119.2	28.10	119.1	0.03	119.2	0.01
HA1-CA-C-N	-59.8	-60.6	27.10	-60.6	26.80	-60.6	26.80	-60.9	0.01	-60.8	0.01
HA2-CA-C-O	-119.2	-119.3	28.40	119.4	28.10	119.2	28.10	119.3	0.03	119.2	0.02
HA2-CA-C-N	60.8	60.6	27.20	60.6	26.80	60.8	26.80	60.7	0.02	60.8	0.01
HA3-CA-C-O	0.0	0.0	27.90	0.0	27.50	0.0	27.60	0.0	0.01	0.0	0.01
HA3-CA-C-N	180.0	180.0	26.70	180.0	26.30	180.0	26.30	180.0	0.04	180.0	0.05
CA-C-N-HN1	0.0	0.0	18.70	0.0	1.10	0.0	1.10	0.0	0.01	0.0	0.01
CA-C-N-HN2	180.0	180.0	16.40	180.0	1.40	180.0	1.40	180.0	0.04	180.0	0.01
O-C-N-HN1	180.0	180.0	19.40	180.0	2.30	180.0	2.30	180.0	0.06	180.0	0.02
O-C-N-HN2	0.0	0.0	15.70	0.0	0.20	0.0	0.20	0.0	0.01	0.0	0.01
out of plane											
C	180.0	180.0	7.40	180.0	1.20	180.0	1.20	180.0	0.02	180.0	0.05
N	180.0	180.0	32.80	180.0	3.00	180.0	3.00	180.0	0.02	180.0	0.04

[a] Bond lengths are in angstroms and angles in degrees. [b] Numbers in parentheses indicate the frequency range retained after filtering (in reciprocal centimeters). [c] Experimental values:[39] CA-C, C-O, C-N 1.53, 1.22, 1.30 Å; CA-C-O, CA-C-N, O-C-N -122, 113, and 125°.

5 ps yielded a maximum frequency of 3335 cm^{-1}, below the N-H stretch frequencies. The observed phenomenon in this case is the aliasing, or "folding", of the high frequencies to a position below the maximum frequency. The folded position of the frequencies above the maximum frequency is given by $\nu_{folded} = \nu_{max} - (\nu_{real} - \nu_{max})$. In Figure 2b–d, the CH as well as the NH stretch frequencies are below the maximum frequency, and in Figure 2f, the CO stretch mode is aliased as well. Although aliasing results in a distorted frequency distribution, it would not, in general, cause significant problems in analyzing the frequency content of the trajectory or for filtering. Since the correct region for the NH, CH, and CO stretches is known, the existence of aliasing can easily be detected. In addition, at the low-frequency region the amplitude of the aliased frequencies is very low and will therefore be negligible when a low-pass filter is applied. It should be noted, however, that the characteristic frequencies of energy properties are twice those of the corresponding structural properties.[24] Thus, a higher sampling frequency is required to reveal all the energy frequencies.

In conclusion, the longer the simulation the better will be the frequency resolution, and modes with very low frequency will be detectable. A long simulation will also minimize the leakage problem. The maximum sampling frequency required for revealing all frequencies of structural properties is 4 ps. However, for the purposes of low-pass filtering, less frequent sampling is sufficient if care is taken in the interpretation of the results.

Low-Pass and High-Pass Filtering of Normal-Mode Trajectories. In order to evaluate the ability of the filtering method to extract selected modes of motion we applied a low-pass filter (ν_{max} = 170 cm^{-1}) and a high-pass filter (ν_{min} = 3200 cm^{-1}) to the trajectory of all normal modes of acetamide. The filtered trajectories were then compared to a trajectory containing only normal mode 21 (the lowest frequency mode) and to a trajectory containing modes 1 and 2 (the two highest frequency modes). Table II characterizes the geometry and mobility of acetamide in the five trajectories, in terms of average values and standard deviations of the internal coordinates. The table also includes the minimized geometry for comparison. A representative section of each of the trajectories of some of the bonds, valence angles, torsion angles, and out of plane angles is given in Figure 3. The corresponding FT of the internals are given in Figure 4.

The average geometry in the trajectory of all normal modes is very similar to the minimum-energy structure (Table II), as is to be expected since the normal modes represent oscillations around a minimum-energy structure. The standard deviations in most bonds are ≈0.02–0.05 Å, and angles deviate 3–5°. The standard deviations of the torsions and out of plane angles range from only 7° to nearly 30°. This is due to the fact that a smaller distortion is required for a high-frequency oscillation to result in the same potential energy contribution as a low-frequency oscillation (see eq 4).

The fluctuations in the internals, as seen in Figure 3, are usually complex in nature, since each internal is involved in more then one normal mode of motion. The FT of the internals, shown in Figure 4, are easier to interpret since they reveal the various frequency components in the oscillations of the internals. The frequencies obtained for each of the internals are consistent with the assignment of the underlying normal modes (Table I). Thus, the NH bonds have two frequency components at ≈3500 cm^{-1}, corresponding to the symmetric and asymmetric NH stretch modes, and the C=O bond has a major component at ≈1650 cm^{-1}, in agreement with normal mode 6, ν(CO). The angle bends of the heavy atoms have major frequency components at the 400–550-cm^{-1} region, in accord with the assignment of normal modes

Table III. Geometry and Mobility of Acetamide (Molecular Dynamics)[a]

	no transitions										with transitions			
			filtered (0–170)[b]				filtered (>3200)[b]							
	original trajectory		coordinates		internals		coordinates		internals		original trajectory		filtered (0–170)	
internal	⟨P⟩	σ	⟨P⟩	σ	⟨P⟩	σ	⟨P⟩	σ	⟨P⟩	σ	⟨P⟩	σ	⟨P⟩	σ
bonds														
CA–HA1	1.109	0.033	1.103	0.007	1.109	0.003	1.072	0.000	1.109	0.000	1.109	0.033	1.103	0.012
CA–HA2	1.110	0.038	1.104	0.007	1.110	0.003	1.073	0.000	1.110	0.001	1.109	0.032	1.103	0.012
CA–HA3	1.109	0.032	1.103	0.007	1.109	0.002	1.071	0.000	1.109	0.000	1.109	0.033	1.103	0.012
CA–C	1.510	0.045	1.508	0.003	1.510	0.003	1.507	0.000	1.509	0.000	1.509	0.039	1.507	0.003
C–O	1.226	0.024	1.223	0.002	1.226	0.001	1.223	0.000	1.224	0.000	1.226	0.028	1.224	0.003
C–N	1.312	0.035	1.310	0.002	1.312	0.001	1.310	0.001	1.309	0.001	1.312	0.033	1.310	0.002
N–HN1	1.025	0.023	0.985	0.031	1.025	0.013	0.983	0.021	0.971	0.022	1.025	0.024	0.986	0.032
N–HN2	1.025	0.026	0.988	0.028	1.027	0.014	0.987	0.024	0.968	0.026	1.028	0.027	0.990	0.028
angles														
HA1–CA–HA2	106.9	5.52	107.1	0.37	106.9	0.23	106.4	0.03	106.9	0.03	107.1	5.32	107.3	0.63
HA1–CA–HA3	108.3	5.54	108.5	0.32	108.3	0.20	107.9	0.03	108.3	0.02	107.5	5.47	107.7	0.68
HA1–CA–C	111.7	4.54	111.8	0.74	111.7	0.74	112.4	0.04	111.7	0.04	111.4	4.96	111.5	1.28
HA2–CA–HA3	106.9	5.54	107.1	0.39	106.9	0.23	106.4	0.04	106.9	0.03	107.2	5.45	107.4	0.63
HA2–CA–C	110.3	4.90	110.3	0.25	110.3	0.20	111.0	0.04	110.3	0.02	111.1	4.83	111.1	1.25
HA3–CA–C	111.7	4.44	111.8	0.75	111.7	0.75	112.4	0.01	111.7	0.02	111.6	4.78	111.6	1.35
CA–C–O	122.2	3.45	122.4	0.16	122.2	0.22	122.4	0.01	122.2	0.02	122.0	3.38	122.2	0.25
CA–C–N	117.3	3.54	117.4	0.24	117.3	0.30	117.4	0.04	117.3	0.04	117.6	3.69	117.7	0.38
O–C–N	120.0	3.50	120.2	0.16	120.0	0.13	120.1	0.06	120.0	0.04	119.9	3.32	120.1	0.20
C–N–HN1	114.9	5.25	116.1	1.22	114.9	1.08	116.1	0.13	114.9	0.11	115.1	5.42	116.3	1.15
C–N–HN2	112.2	5.56	112.9	1.07	112.2	1.09	113.0	0.11	112.2	0.10	112.3	5.56	113.1	1.07
HN1–N–HN2	127.3	4.75	130.8	2.01	127.3	1.12	131.0	0.18	127.3	0.18	127.4	4.66	130.5	1.92
torsions														
HA1–CA–C–O	−119.0	17.31	−119.0	16.22	−119.0	16.24	−119.0	0.03	−119.1	0.03	110.1	379.10	110.1	379.00
HA1–CA–C–N	61.0	16.57	61.0	15.63	61.0	15.67	60.9	0.03	60.9	0.03	290.1	379.00	290.1	379.00
HA2–CA–C–O	0.0	16.85	0.0	15.86	0.0	15.90	0.0	0.03	0.0	0.02	229.8	379.00	229.7	378.90
HA2–CA–C–N	180.0	16.27	180.0	15.28	180.0	15.34	180.0	0.03	180.0	0.02	409.8	378.90	409.7	378.90
HA3–CA–C–O	119.1	17.29	119.1	16.19	119.1	16.21	119.0	0.03	119.0	0.01	349.7	379.00	349.6	378.90
HA3–CA–C–N	−60.9	16.56	−60.9	15.61	−60.9	15.64	−61.1	0.03	−61.0	0.03	169.7	379.00	169.6	378.90
CA–C–N–HN1	0.0	17.99	0.0	2.16	0.0	2.21	0.0	0.21	0.0	0.05	0.0	17.90	0.0	2.40
CA–C–N–HN2	180.0	17.80	180.0	1.84	180.0	1.88	180.0	0.14	180.0	0.05	180.0	17.20	180.0	1.90
O–C–N–HN1	180.0	18.34	180.0	2.40	180.0	2.45	180.0	0.19	180.0	0.05	180.0	17.90	180.0	2.70
O–C–N–HN2	0.0	15.77	0.0	1.58	0.0	1.64	0.0	0.15	0.0	0.04	0.0	15.80	0.0	1.60
out of plane														
C	180.0	8.55	180.0	0.72	180.0	0.85	180.0	0.02	180.0	0.04	180.0	8.60	180.0	0.80
N	180.2	28.50	180.2	4.32	180.2	4.33	180.2	0.38	180.2	0.07	180.0	27.30	180.0	4.60

[a] Bond lengths are in angstroms and angles in degrees. [b] See footnote *b* Table II.

Table IV. Geometry and Mobility of *N*-Acetylalanine-*N'*-methylamide. Molecular Dynamics Trajectory[a]

	minimized		original trajectory		filtered (0–70)[b]	
internal	C_7^{eq}	α_R	⟨P⟩	σ	⟨P⟩	σ
bonds						
CC–C1	1.504	1.505	1.512	0.035	1.512	0.002
C1–O1	1.229	1.227	1.231	0.025	1.231	0.001
C1–N1	1.328	1.327	1.333	0.031	1.333	0.002
N1–CA	1.484	1.487	1.491	0.033	1.491	0.003
CA–C2	1.564	1.569	1.574	0.041	1.574	0.005
CA–CB	1.538	1.540	1.547	0.037	1.547	0.004
C2–O2	1.234	1.233	1.237	0.023	1.237	0.001
C2–N2	1.342	1.344	1.347	0.031	1.347	0.002
N2–CN	1.469	1.469	1.476	0.032	1.476	0.003
angles						
CC–C1–O1	120.9	120.8	120.4	3.18	120.4	0.33
CC–C1–N1	115.2	115.0	115.2	3.29	115.2	0.44
O1–C1–N1	123.8	124.2	123.9	2.93	123.9	0.32
C1–N1–CA	122.6	122.6	122.7	2.57	122.7	0.39
N1–CA–C2	113.5	118.1	113.2	4.09	113.2	2.30
N1–CA–CB	105.9	106.1	106.4	3.81	106.4	1.22
C2–CA–CB	113.4	112.2	112.4	3.64	112.4	1.16
CA–C2–O2	121.6	118.5	120.9	3.08	121.0	0.72
CA–C2–N2	119.1	122.0	116.5	3.10	116.5	0.85
O2–C2–N2	122.4	122.0	122.2	2.80	122.2	0.39
C2–N2–CN	122.1	122.0	122.2	2.49	122.2	0.39
torsions						
CC–C1–N1–CA	179.7	182.1	178.8	11.00	178.8	9.30
C1–N1–CA–C2	−86.0	−78.5	−102.5	24.60	102.5	23.90
N1–CA–C2–N2	83.7	−33.9	92.0	43.10	92.0	42.80
CA–C2–N2–CN	180.8	179.1	180.0	10.50	180.0	5.10

[a] Bond lengths are in angstroms and angles in degrees. [b] See footnote *b* Table II.

17 and 18. The two torsions and two out of plane angles have four frequency components: at ≈90, 250, 430, and 550 cm^{-1}. The torsion around CA–C has a major component, at ≈100 cm^{-1}, and a small component at ≈550 cm^{-1}. This can be seen from the trajectory plot as well (Figure 3), where a relatively high frequency and small amplitude vibration is superimposed on a low-frequency

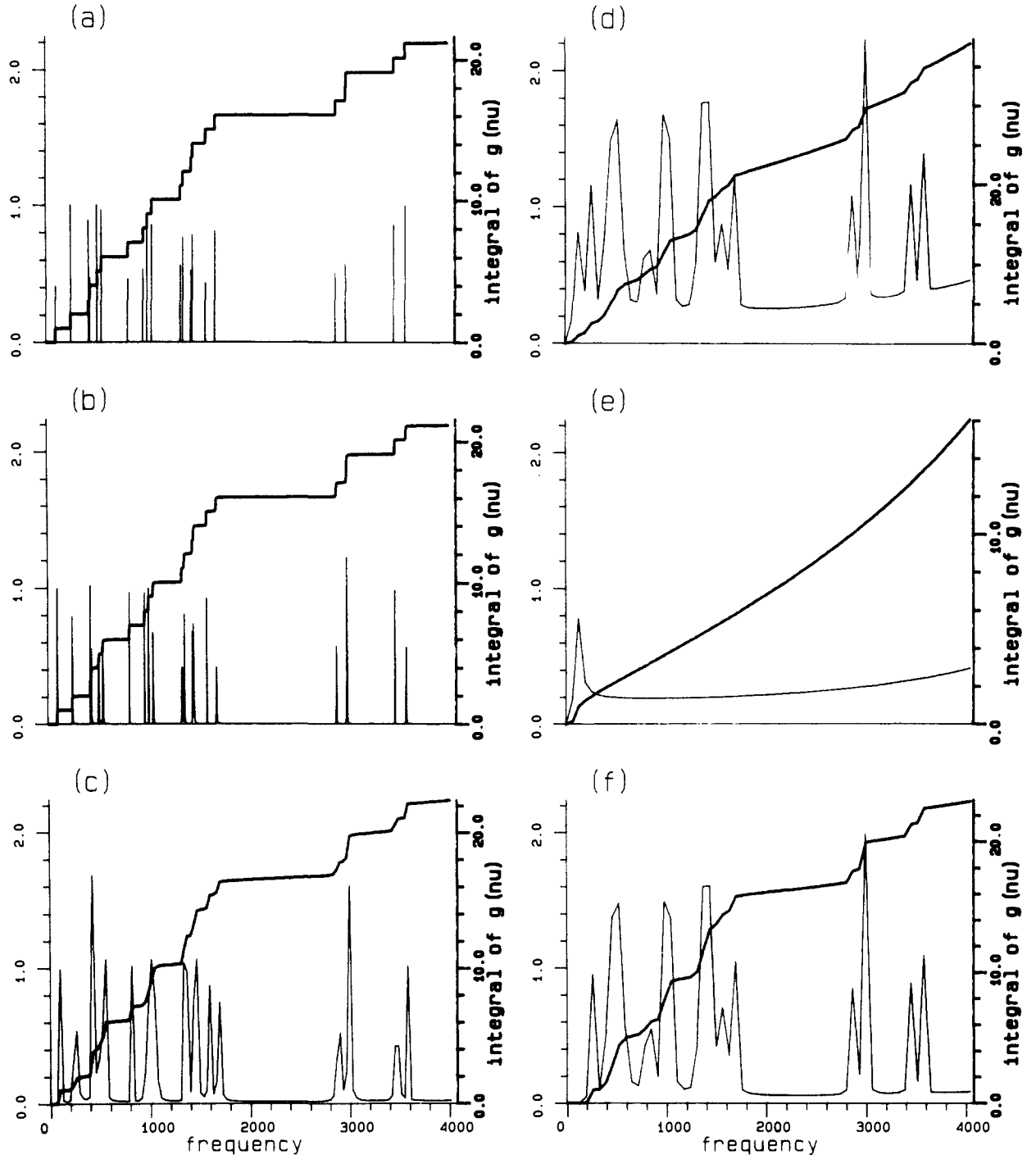

Figure 1. Frequency distribution of a normal-mode trajectory of acetamide as a function of simulation length, demonstrating the phenomenon of "leaking". The simulation length is 64, 8, 1, and 0.5 ps in sections a–d. Sections e and f correspond to a 0.5-ps simulation of normal mode 21 only and normal modes 1–20, respectively. (Frequencies are in reciprocal centimeters.)

and high-amplitude vibration. Similarly, the out of plane deformation around the nitrogen has a major low-frequency oscillation and a higher frequency small amplitude superimposed on it. The two frequencies involved here are 250 and 550 cm^{-1}, as revealed by the FT diagram. The rotation around the amide bond has almost equal components at ≈250 and 430 cm^{-1}, and the out of plane deformation of the carbonyl has a major component, although of low amplitude, at ≈550 cm^{-1}. This is in accord with the normal-mode assignment of frequencies 16 and 19–21, in Table I.

The only discrepancy in average structure and mobility involves the hydrogen atoms, which have extended bond lengths and some deviations in valence angles (Table II), as well as an apparent low-frequency motion (Figures 3 and 4). The origin of this deviation is in the process of generating the normal-mode trajectory. This was done in Cartesian space, and thus motions, that should describe circular movement (e.g., a torsion) are actually linear along a tangent to the circle, and for fluctuations that are not infinitesimally small, this leads to distortion. This can be seen in the bond trajectory plots in Figure 3, and the corresponding FT of the bonds in Figure 4. In addition to the high-frequency in the CH and NH bonds (≈3000 and ≈3500 cm^{-1}, respectively), a low-frequency oscillation is present due to distortions accompanying the torsional vibrations. This will have no effect on the evaluation of the filtering technique, since for this purpose we only need to know what motions are in the trajectory before and after the filter and not if they accurately represent normal-mode motion.

The results of the low-pass filter are summarized in Table II, and trajectory plots and corresponding FT are depicted in the second column of Figures 3 and 4. All bond and angle vibrations

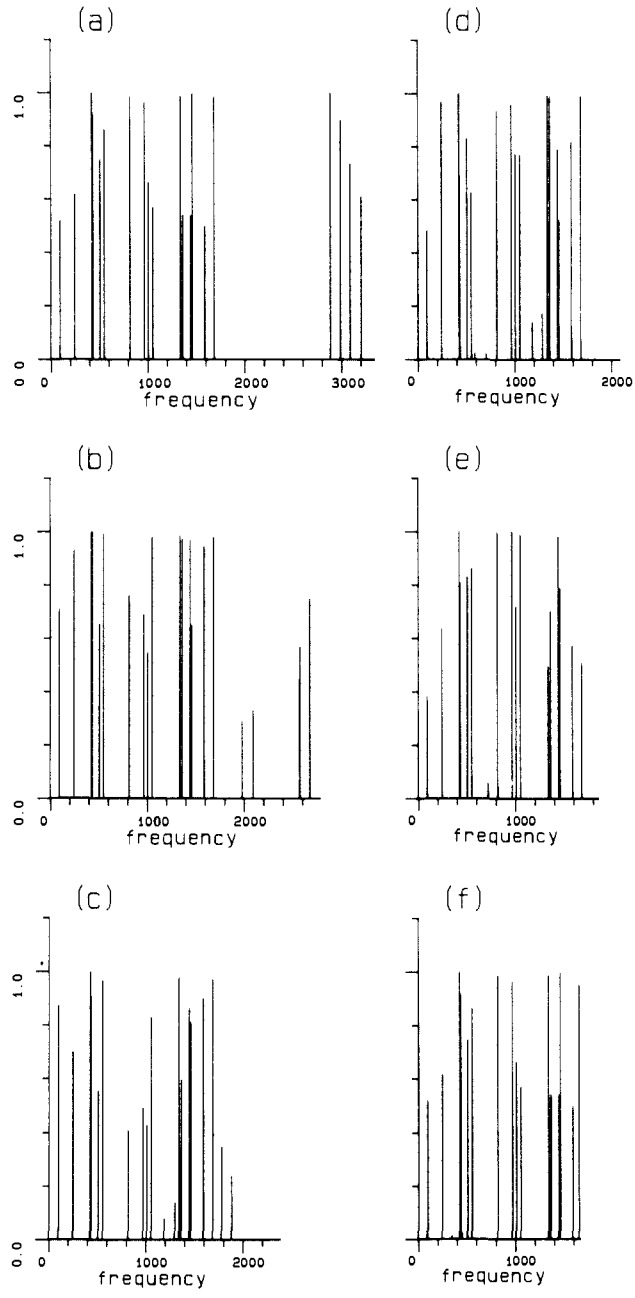

Figure 2. Frequency distribution of a normal-mode trajectory of acetamide as a function of sampling frequency, demonstrating the phenomenon of "aliasing". The frequency of sampling is 5–10 ps in sections a–f, respectively. (Frequencies are in reciprocal centimeters.)

(except those involving the methyl hydrogens) were eliminated. The standard deviations of the amide torsion and the two out of plane angles were reduced to ≈1–3°, whereas the standard deviation of the CA–C torsion was basically unaltered. Thus, the filtering resulted in the removal of most motion except the CA–C torsion. Even more significant is the similarity of the resultant motion to the motion obtained from a normal-mode trajectory containing only normal mode 21. Both the average and the standard deviation of the internals are identical in the two trajectories. Comparison of the corresponding trajectory plots and FT reveals again the close similarity between the two trajectories in frequency, amplitude, and phase of the fluctuations in the internals. Note that the low-frequency motion of the CH bond and the HCC and HCH valence angles is present in *both the filtered and the single normal-mode trajectory*. Although in general the filtered trajectory is nearly identical with the trajectory of the single normal mode, some distortions are observed at the "edges" of the filtered trajectory. For example, the first ≈0.1 ps of the CA–C torsion does not look similar to the overall shape

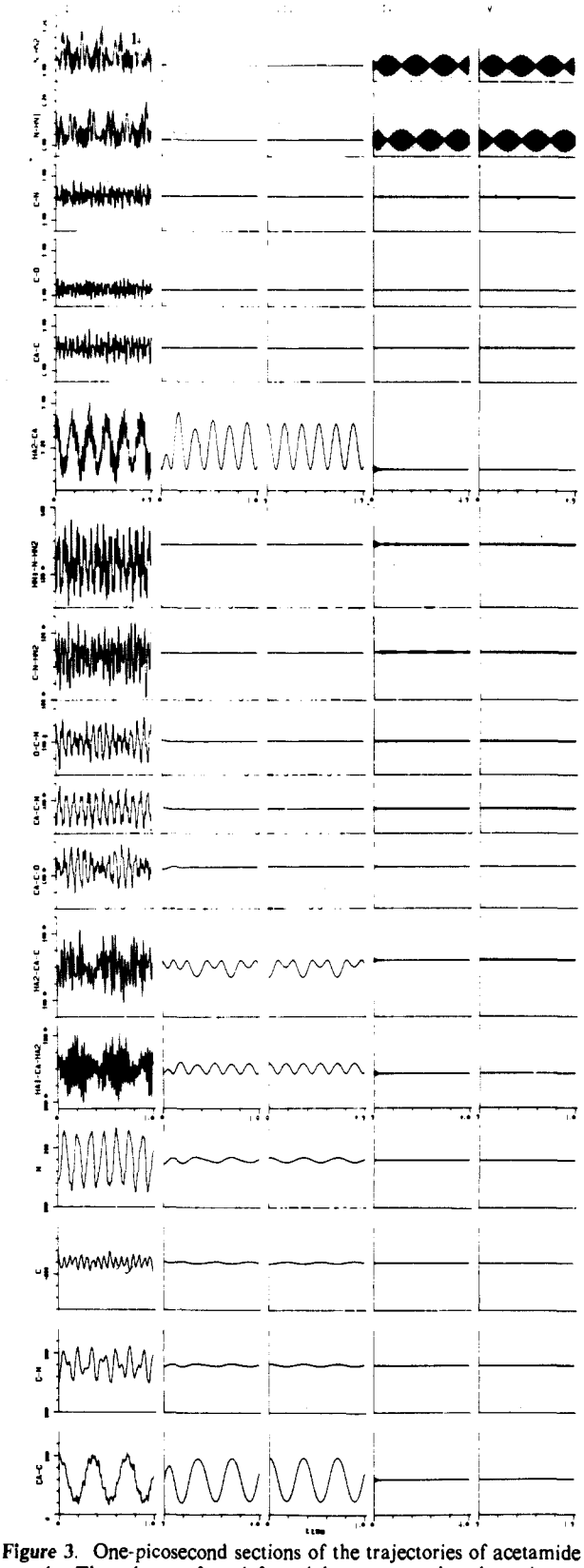

Figure 3. One-picosecond sections of the trajectories of acetamide internals. The columns, from left to right, correspond to the trajectory of all normal modes, a low-pass-filtered trajectory, a trajectory of normal mode 21 only, a high-pass-filtered trajectory, and a trajectory of normal modes 1 and 2 only. The rows, from top to bottom, correspond to bonds, valence angles, out of plane angles, and torsion angles. (Bonds are in angstroms, angles are in degrees, and time is in picoseconds.)

of this section in the original trajectory or in the trajectory of a single normal mode. This is due to the finite length of the simulation, which does not necessarily correspond to an integral multiple of the periods of the various oscillations. We have seen

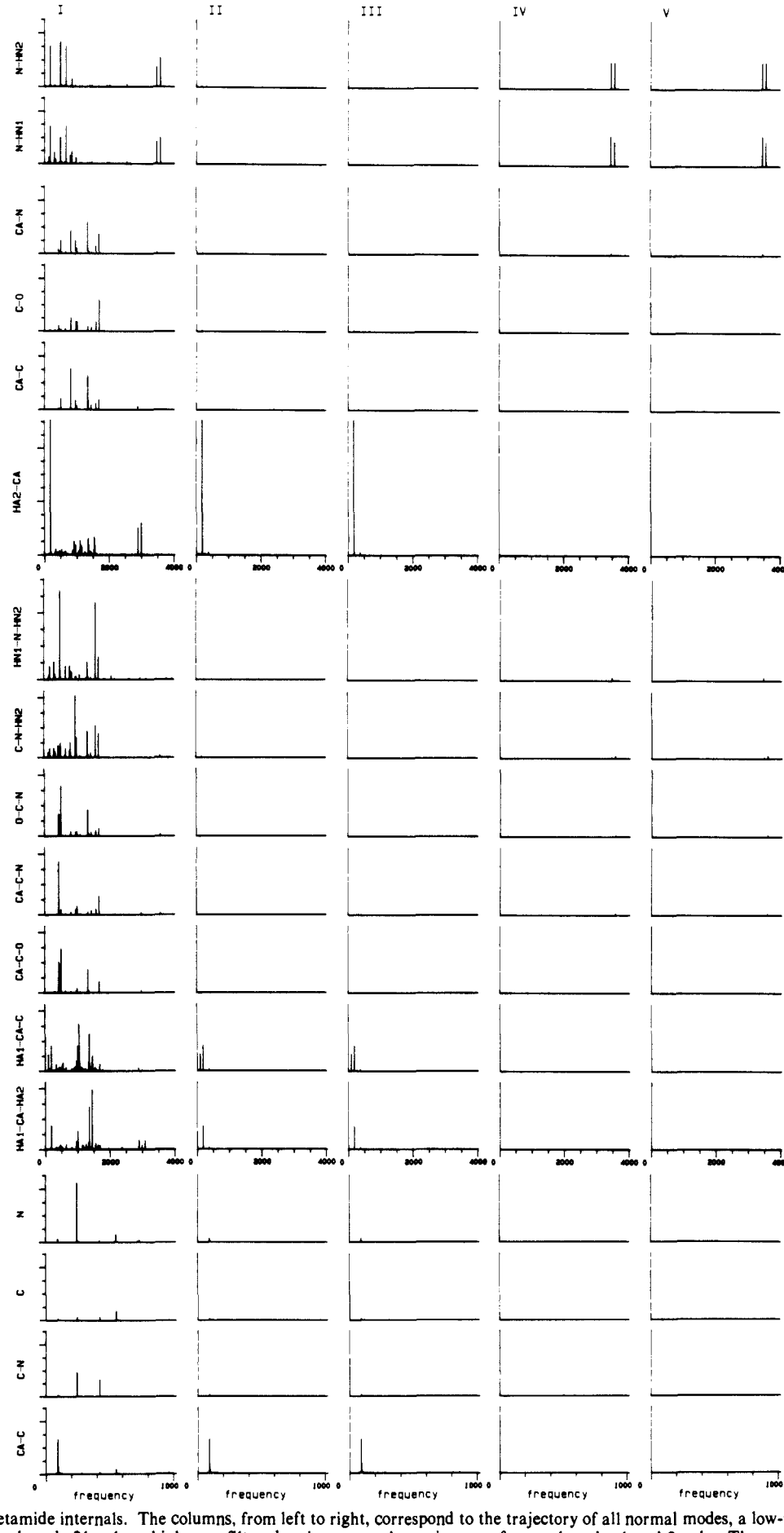

Figure 4. FT of acetamide internals. The columns, from left to right, correspond to the trajectory of all normal modes, a low-pass filtered trajectory, a trajectory of normal mode 21 only, a high-pass-filtered trajectory, and a trajectory of normal modes 1 and 2 only. The rows, from top to bottom, correspond to bonds, valence angles, out of plane angles, and torsion angles. (Frequencies are in reciprocal centimeters.)

that this truncation results in the leakage phenomenon upon Fourier transformation. Applying the inverse FT introduces analogous distortions to the resulting time domain function, which is made to look like a multiple of a wave function period (i.e., the end and the beginning values of the filtered coordinate have the same value). This distortion is of a very limited duration, of less then 0.2 ps, and the rest of the filtered trajectory follows the corresponding single normal-mode trajectory very closely in terms of amplitude, phase, and frequency.

A similar analysis was carried out on the effects of applying a high-pass filter to the normal-mode trajectory. The filtering function was chosen so as to retain the two NH stretch modes, i.e., $\nu_{min} = 3200\ cm^{-1}$. The results were compared to a normal-mode trajectory, which was generated by using a superposition of only two normal modes, the symmetric and asymmetric NH stretches (modes 1 and 2 in Table I). As seen from Table II, the only bond vibrations retained after filtering were the NH bonds. Most of the valence angle vibrations (except for very small vibrations involving the NH group) and all torsion and out of plane vibrations were eliminated. The trajectories of the two NH bonds in the original all normal-modes trajectory (Figure 3) is another example of a complex motion. These bonds are involved in quite a few vibrations in addition to the obvious high-frequency NH stretches. Again, the understanding of the motion of the NH bonds is greatly assisted by the FT given in Figure 4. The expected pair of frequency components is seen at $\approx 3500\ cm^{-1}$, but a myriad of low-frequency components is observed as well, accounting for the very complex appearance of the time domain trajectory. After filtering, all the low-frequency components disappeared, leaving only the two components at $\approx 3500\ cm^{-1}$ nearly identical with the frequency distribution for the NH stretches in the trajectory of normal modes 1 and 2 only (Figure 4). The combination of two NH vibrations of similar frequency leads to a typical trajectory of "beating", in which the maximum NH stretch goes from 0 (when the two modes cancel each other) to double the amplitude of a single vibration (when the two modes add up). The trajectories shown in Figure 3 for the trajectory of normal modes 1 and 2 clearly display this behavior. Since the two modes correspond to symmetric and asymmetric vibrations of the two bonds, the "beating" wave is out of phase, when the two modes add up for one bond they cancel for the other. Examining the two NH bond vibrations in the high-pass-filtered trajectory reveals that the filtering process succeeded in extracting this typical beating trajectory out of the very complex "noise-like" behavior in the original trajectory.

In conclusion, the results obtained by applying a low- and a high-pass filter to a trajectory of all normal modes are virtually identical with the corresponding trajectories of only normal mode 21 and normal modes 1 and 2, respectively. This similarity includes frequency phase and amplitude of the vibrations, which account for the total motion, and is exhibited in the similar values of the internal coordinates, their standard deviations, the time dependence trajectory plots, and FT plots. We concluded therefore that for small oscillations around a minimum it is possible to extract the underlying modes of motion by applying the appropriate filtering functions.

Filtering of Molecular Dynamics Trajectories. The success of the filtering technique in extracting selected modes from a normal-mode trajectory is an essential test of the method, but has no practical applications since the extracted modes where known a priori form the normal modes directly. The next stage in the evaluation of the filtering method as a tool in the analysis of molecular dynamics simulations was to apply it to a "real" trajectory. First, a molecular dynamics simulation of acetamide was carried out for comparison with the normal-mode trajectories. In addition, the method was also tested on a small model peptide to examine simple characteristic motions in peptides and proteins. For both molecules some sections of the simulation involved only fluctuations around one minimum, whereas in other sections conformational transitions occurred.

Fluctuations Around One Minimum. A summary of the average structure and mobility of acetamide in a section of the molecular dynamics with no rotations around the CA–C bond is given in Table III. Sections of the trajectories of the internals are given in Figure 5. The corresponding FT are given in Figure 6. The average structure in this trajectory is very similar to the one

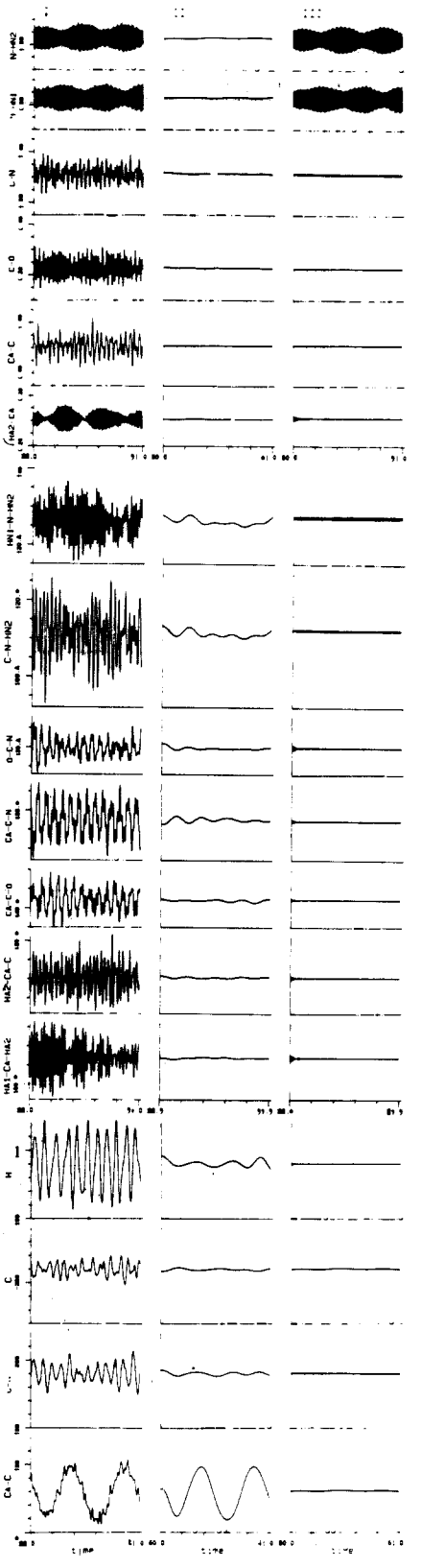

Figure 5. One-picosecond sections of the trajectories of acetamide internals, from a molecular dynamics simulation (no rotations of the CC bond). The left-hand column corresponds to the original trajectory. The next two correspond to a low- and a high-pass filter of the Cartesian coordinates. The rows, from top to bottom, correspond to bonds, valence angles, out of plane angles, and torsion angles. (Bonds are in angstroms, angles are in degrees, and time is in picoseconds.)

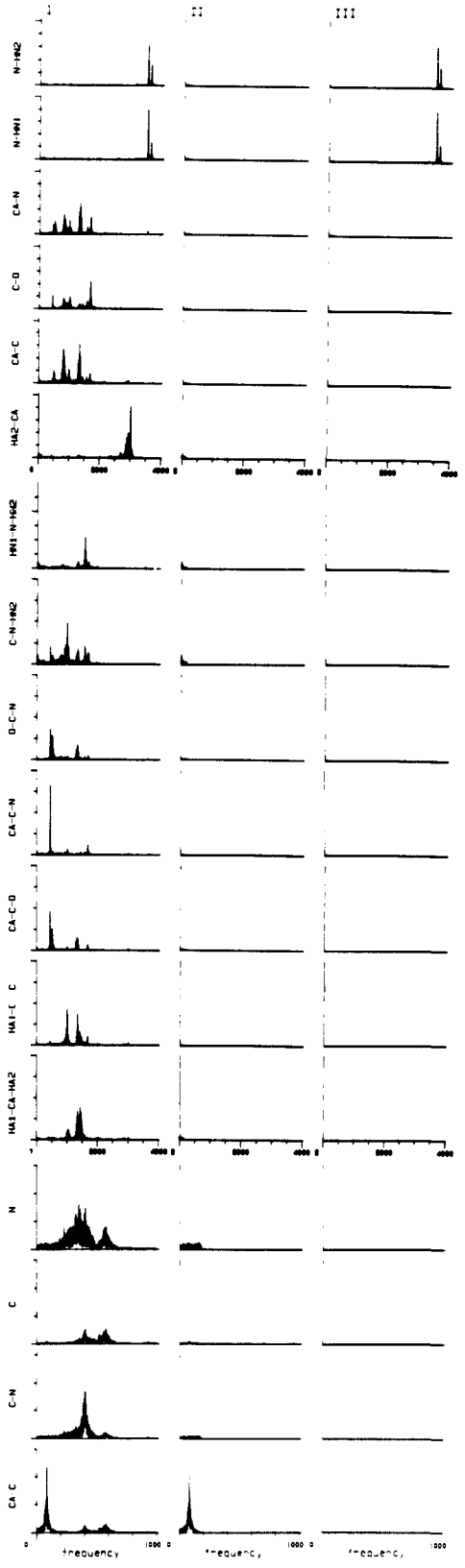

Figure 6. FT of acetamide internals, from a molecular dynamics simulation (no rotations of the CC bond). The left-hand column corresponds to the original trajectory, and the next two correspond to a low- and a high-pass filter of the Cartesian coordinates. The rows, from top to bottom, correspond to bonds, valence angles, out of plane angles, and torsion angles. (Frequencies are in reciprocal centimeters.)

obtained for a normal-mode trajectory (Table II). As mentioned above, some of the bonds and valence angles involving the hydrogen atoms are distorted in the normal-mode trajectory due to the generation of the trajectory in Cartesian space. These distortions are absent from the molecular dynamics trajectory. Note, however, the small deviations in the value of the average internal when calculated from the trajectory of internals, or from the average Cartesian coordinates. The overall mobility is also similar, although the fluctuations in CA–C torsion are smaller in the molecular dynamics simulations.

Comparing the FT of the internals in the molecular dynamics simulation (Figure 6) with those obtained from a normal-mode trajectory (Figure 4) reveals that the oscillation frequencies are very similar but the "peaks" are much broader and have a different pattern of intensities. This is due to the fact that the motion in the normal-modes trajectory is very regular with constant frequencies and amplitudes, whereas the molecular dynamics trajectory is more "chaotic" in nature. A "characteristic" mode of motion can vary during the simulation with respect to the exact frequency due to transient changes in the local environment. The amplitude of a motion varies as well according to the amount of energy in the mode.

In order to evaluate the results of the filtering technique, two methods of calculating the filtered trajectories of the internal were employed. In one method the filter was applied to the Cartesian coordinates and the values of the internals were obtained from the filtered coordinates. The alternative route was to calculate internals first from the unfiltered Cartesian coordinates and then apply the filter to the internals. In general, the results from the two methods were nearly identical, suggesting that the two operations, filtering and calculating the internals, are usually commutative. The main deviation between the results of the two methods occurs for the NH bonds. The effect of averaging the coordinates and then calculating the internals and similarly applying the filter on the coordinates neglects some of the correlated nature of the motion of the nitrogen and the hydrogen atoms, resulting in an apparent shortening of the average bond length.

Table III and Figures 5 and 6 show that the low-pass filter essentially removed all bond and valence angle vibrations, and most of the amide torsion and out of plane angle vibrations. The size of the fluctuations in the CA–C torsion was hardly affected by this filter. This result is very similar to the effect of this filter on the normal-mode trajectory. However, it is worth noting that although the standard deviations in valence angles in the original trajectories are similar, very little of the fluctuations were retained in the filtered molecular dynamics trajectory. This suggests that the frequency components in the original trajectories are quite different. For example, while the normal-mode trajectory contained significant low-frequency components for angles involving the methyl hydrogen atoms, which were retained on filtering, the molecular dynamics trajectory contains mainly higher frequency components.

The high-pass filter results in the elimination of essentially all fluctuations in valence angle, torsion, and out of plane angles. The only motion left is the NH stretch. The familiar beating pattern is observed again, indicating a superposition of two frequency components. But unlike the normal-mode trajectory, the beating is not "perfect" in the sense that complete cancellation (or addition) of the amplitudes does not occur. The difference in pattern is due to that fact that the maximum amplitudes of the symmetric and asymmetric modes are not equal, as demonstrated by the corresponding FT in Figure 6. This is yet another manifestation of the nonequal partitioning of energy into the various modes of motion.

Thus, it is possible to extract typical motions from a molecular dynamics simulation as well as from a normal-mode trajectory. Although the nonregular nature of the motion in molecular dynamics simulations results in broadening of the frequency distribution peaks, a band-pass filter that reflects this broadening will still result in successful filtering. In some cases it may be difficult to resolve types of motion with similar frequencies by filtering; however, it is still possible to select a range of frequencies for filtering and obtain the combined motion corresponding to the spread of frequencies. However, it has been found that at high energies the trajectories are chaotic and the corresponding power spectra are "grassy".[41] The validity of applying the filtering

technique to such systems would require further investigation.

Conformational Transitions. Acetamide. The region 0–65 ps of the molecular dynamics simulation of acetamide was used to examine the applicability of the filtering technique to regions of the potential that are far from the local minimum, including conformational transitions. In this section of the trajectory, the CA–C bond undergoes fluctuations around the minimum-energy conformation as well as full rotations. The averages and standard deviations of the internals in this trajectory and in a low-pass-filtered trajectory are summarized in Table III and compared to the corresponding averages and deviations in the section of the dynamics without transitions (60–93 ps). Obviously, the average and standard deviations of the torsion around the CA–C are different in the original two sections. All other internals are very similar. Applying a low-pass filter to the 0–65 ps retained the values of the Ca–C torsion very close to the unfiltered values. The averages and standard deviations of all other filtered internals are very similar for the two sections. However, larger standard deviations were retained for the angles in the 0–65-ps section, in closer agreement with the results in the normal-mode trajectory. This implies that a larger low-frequency component existed in the angle trajectory in this part of the simulation. It is also consistent with the fact that conformational transitions occur; i.e., large enough fluctuations in the low-frequency CA–C torsional vibrations occurred to cause rotations.

***N*-Acetylalanine-*N'*-methylamide.** The lowest two frequencies, 48 and 62 cm^{-1} for the C_7^{eq} conformation and 30 and 51 cm^{-1} for the α_R conformation, correspond to fluctuations in the torsions ϕ and ψ. The next four modes, 80–165 cm^{-1}, have components of torsions around the blocking methyl groups. Since we were mainly interested in the conformational motion, which is determined by the torsions ϕ and ψ, we chose the low-pass filter with $\nu_{max} = 70$ cm^{-1}.

The average geometry and the mobility of the molecule in the original and filtered trajectory are given in Table IV. For comparison, the minimized geometries for the C_7^{eq} and the α_R conformations are given as well in this table. The two minimized conformations have very similar bond lengths, and most of the angles are within 0.5°. However, the CA–C2–N2, CA–C2–O2, C2–CA–CB and, in particular, N1–CA–C2 angles differ significantly (2–5°). The average values of the internals in the original and filtered trajectories are very similar. The average bond lengths in the simulation are consistently larger than the corresponding values in either of the two minimized conformations. This indicates that it is easier to stretch the bonds than to compress them, which is in accord with the asymmetric form of the Morse potential. This phenomenon is well known in experimental determinations of structure by electron diffraction, where the measurements result in longer bond lengths for higher temperatures. The average values for the valence angles are close to the minimized values. For the angles that depend on the conformation, the average values in the dynamics are between the values of the minimized C_7^{eq} and the α_R conformations. (Closer to the first conformation, which exists for longer periods of the simulation.) The average values of ϕ and ψ are not in the range defined by the two minimized conformations due to large fluctuations toward regions other then the path between the C_7^{eq} and α_R minima.

The standard deviations in the values of the internals in the original trajectory were similar to those obtained for acetamide. On filtering, the fluctuations in bonds virtually disappeared. The fluctuations in the two ω torsions were reduced, but the standard deviations in ϕ and ψ remained almost unchanged. The fluctuations in valence angles were greatly reduced on filtering, but not removed completely. In particular, angles involving the CA as a central atom deviate by ≈10–20°, and angles involving the C2 as a central atom deviate up to ≈6°. The fluctuations in torsion angles ϕ, ψ as well as those of the four angles that depend on conformation are given in Figure 7 for the original and filtered trajectory. It is obvious from this figure that the low-frequency motion of the molecule involves changes in torsion angles as well as distortions of valence angles. It is particularly apparent that the changes in conformation are not limited to changes in torsion angles but coupled changes in valence angles occur as well. However, in the original trajectory it is difficult to detect the changes in valence angles associated with the low-frequency conformational motion, due to the superimposed large-amplitude high-frequency fluctuations. In the filtered trajectory, on the other hand, it is easy to see that each transition from C_7^{eq} to α_R, as indicated by a change of ψ from ≈80° to ≈−50°, is accompanied by changes of valence angles. For example, the CA–C2–O2 angle changes from ≈121° to ≈118° and the CA–C2–N2 angle changes from ≈116° to ≈120°. These values are consistent with the values obtained for the two minimized conformations. Thus, we see again that the study of conformational mobility has to take into account not only torsional degrees of freedom but also changes in valence angles. In order to convey the overall nature of the conformational changes, we depict in Figure 8 a series of "snapshots" of the molecule in the original and filtered trajectories, 0.1 ps apart. While the general appearance of the transitions in the two trajectories is very similar, large local distortions are observed in the original trajectory while the transition in the filtered trajectory appears smooth. This reflects a general feature of filtering molecular dynamics trajectories—it is possible to display "frames" at large intervals without apparent "jerkiness", and thus the faster display of slow processes is possible.

Computational Requirements. The most demanding part of the filtering technique, in terms of computer resources, is the generation of the trajectories, i.e., the molecular dynamics simulation. The CPU time required for each time step depends mainly on the number of nonbonded interactions, which is proportional to the square of the number of atoms, N. The memory requirement and disk/tape storage allocation depend linearly on N. Obviously, the amount of CPU time and storage will increase (linearly) with the length of the simulation. For the *N*-acetylalanine-*N'*-methylamide molecule a 133-ps simulation took ≈33 h of CPU time on a microVAX II, and generated ≈90 Mbytes of history files, including coordinates, velocities, and energies. The filtering stage is much less intensive in computing. In order to perform the FT of the coordinate trajectories it is necessary to have all time steps of a coordinate simultaneously, whereas in the trajectory generated during the simulation all coordinates of one time step are grouped together. Thus, the coordinates have to be rearranged prior to the filtering. Reordering of all the coordinates (3 × 22) of the whole trajectory of the blocked alanine took 14 min and generated a file of 8.7 Mbytes. To reorder the whole trajectory in one step would have required 8.7 Mbytes of virtual memory. Instead, we allocated only 4 Mbytes, and the process was carried out in stages, a section of the trajectory at a time. The dependence of the fast FT on the number of time steps is $\approx n \log n$. Fourier transforming all the coordinates to the frequency domain, applying the filtering function, and inverse Fourier transforming back to the time domain required 25 min. Since each coordinate is filtered independently, the process of filtering is highly modular and can be adapted to the size of the system and the available resources. (See ref 23 for the computer requirements for filtering a trajectory of a protein.)

Conclusions

We have described a new technique for analyzing and interpreting molecular dynamics simulations and demonstrated its application to small molecules as models for peptides and proteins. The method is based on a Fourier analysis of the atomic trajectories to define the characteristic modes of motion, in terms of frequency and amplitude. A filtering function is applied to select only the motions of interest, and an inverse FT regenerates the time domain trajectories that include only the selected motions. The effect of filtering was examined qualitatively by displaying the original and filtered trajectories on an interactive display system.[42] Quantitative comparison were carried out by examining

(41) Dumont, R. S.; Brumer, P. *J. Chem. Phys.* **1988**, *88*, 1481–1496.

(42) A video comparing the original and filtered trajectories (normal mode and molecular dynamics) of alanine, and of the protein phospholipase A_2 is available from the authors upon request.

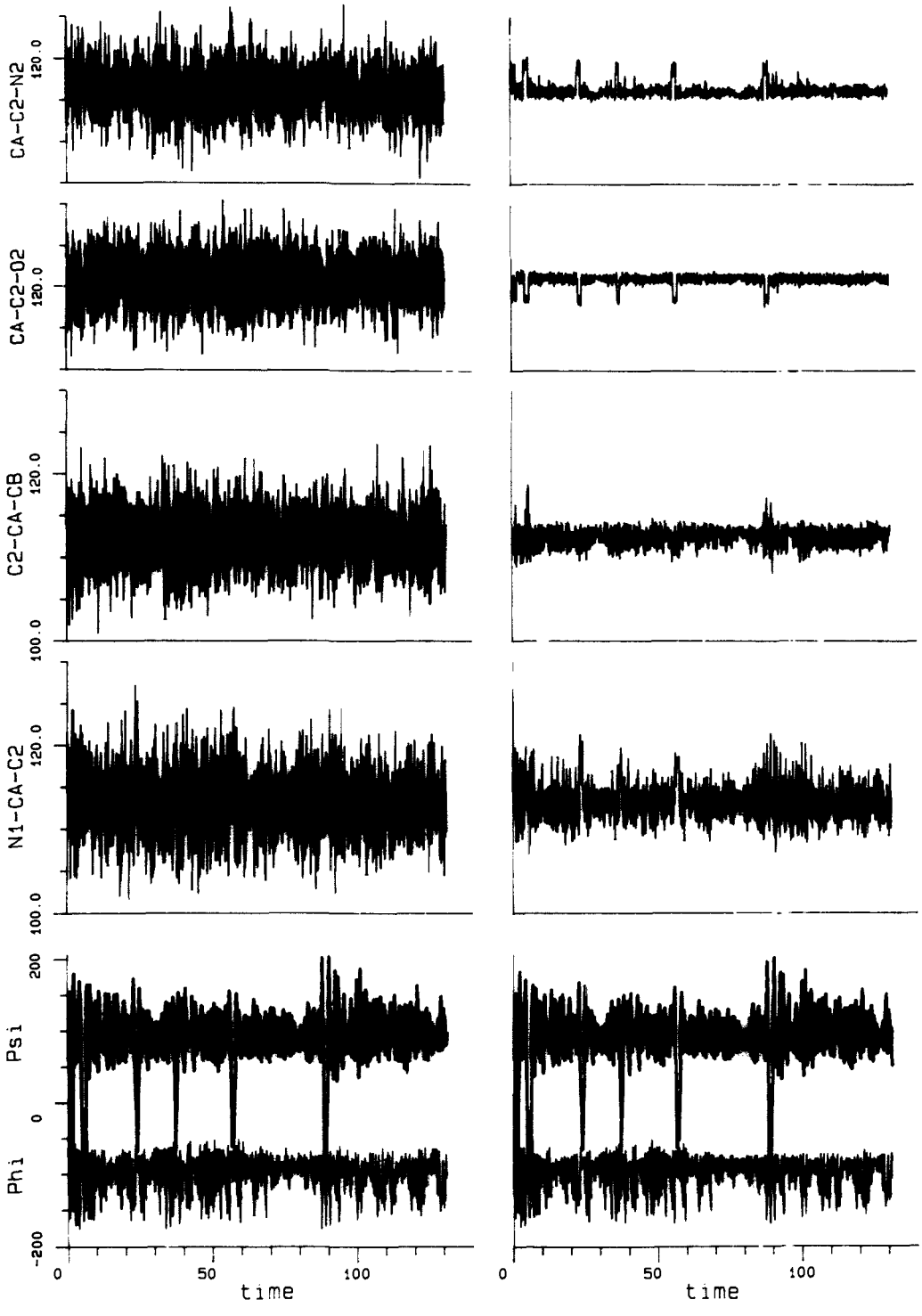

Figure 7. Trajectories of ϕ, ψ and the valence angles N1–CA–C2, C2–CA–CB, CA–C2–O2, and CA–C2–N2 of *N*-acetylalanine-*N'*-methylamide. The original trajectories are given on the left and the filtered trajectories on the right. (Angles are in degrees, and time is in picoseconds.)

the time averages, standard deviations, and frequency distribution of the internal coordinates. As evident from applying the filtering technique to "normal-mode trajectories", the filtered trajectories have all the characteristics of the original modes that have frequencies in the selected range. Applying the method to molecular dynamics simulations was equally successful. We concluded that it is possible to extract the individual components of motion or a combination of a number of motions from a trajectory. Thus, this technique is an important tool in partitioning the overall motion into the underlying characteristic modes. It provides information similar to that obtained from normal-mode analysis, but has the added advantage of being applicable in regions far from the local minima, including anharmonic regions and conformational transitions.

The filtering method is very flexible in its application and is not very demanding in computer resources. Selecting different modes of motion is achieved by designing the appropriate filtering function, and particular parts of the molecule can be focused on by including only the corresponding atoms in the filtering process. It can be applied to the Cartesian coordinates directly or to any property that can be calculated from these coordinates, such as internal coordinates, interatomic distances, radius of gyration, moments of inertia, etc. Although some distortions in bond length can result when low-pass filtering is done in Cartesian coordinates, conformational motion, as defined by the torsion angles, is represented equally well when the filtering is applied to the Cartesian coordinates or to the torsion angles directly. The rate-determining step in the filtering process is the generation of the trajectories.

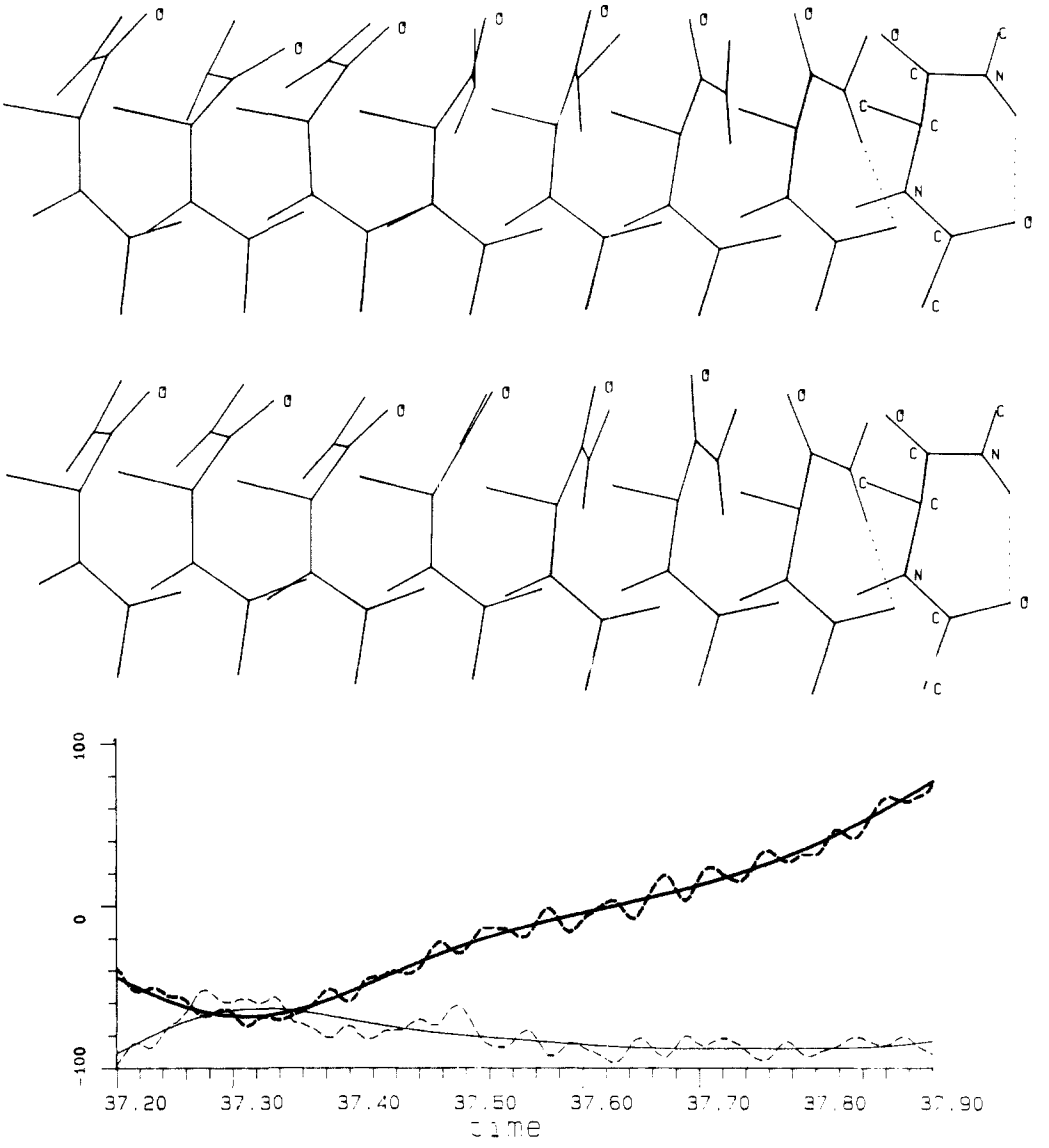

Figure 8. One of the conformational transitions ($\alpha_R \rightarrow C_7^{eq}$) occurring during the molecular dynamics simulation of *N*-acetylalanine-*N'*-methylamide. A section of the trajectory of ϕ (thin lines) and ψ (thick lines) is shown at the bottom, with full and dashed lines representing the original and filtered trajectories, respectively. Two sequences of transient structures are shown above the torsion trajectory at corresponding times (at intervals of 0.1 ps). The top sequence is taken from the original trajectory and the bottom sequence is from the filtered trajectories. (Angles are in degrees, and time is in picoseconds.)

Although this can be quite demanding in CPU time and storage allocation, particularly for long simulations and/or large systems, current computer power enabled numerous applications even to large protein systems.[13] The filtering step itself is much less demanding, as discussed above, and since each coordinate is processed independently, filtering can be carried out in several steps if resources are limited. In contrast, normal-mode analysis requires *full* minimization prior to the analysis, calculation, storage, and inversion of a second-derivative matrix, which are expensive in CPU and memory allocation. Thus, the application of normal-mode calculations to large systems was up to now very limited and required additional approximations such as rigid geometry or partial minimization.[20-22] These approximations are not necessary when applying the filtering technique.

Of particular interest is the ability to filter out all high-frequency bond and angle fluctuations and focus on the low-frequency conformational motions. In fact, it is nearly impossible to study the conformational motion in the original trajectories because of the superimposed high frequencies. One of the most basic ways to examine the results of a molecular dynamics trajectory is by visual inspection on a graphic display system. However, the use of this method for the analysis of conformational motion is usually hindered by the long time scale of conformational events and the distracting nature of the superimposed high-frequency motion. Increasing the rate of display causes blurry pictures, while skipping frames results in jerky motion. On the other hand, in a low-pass filtered trajectory, all high-frequency motions are removed and thus the display of conformational motion is much easier and meaningful. Any other method of analysis of the conformational motion, such as trajectories of internals for example, is similarly hindered by the high-frequency motion. As we have shown, changes in valence angles associated with conformational transitions, for example, could only be detected after applying the appropriate filter.

Applying a low-pass filter is especially useful for studying conformational transitions. We have shown for the alanine dipeptide that the general features of the conformational transitions are maintained after filtering. However, the local transient bond and angle distortions due to high-frequency oscillations disappeared, thus enabling us to concentrate on and reveal the characteristics of the transition path. It is important to emphasize that the filtering process does not necessarily result in fixed bond lengths and valence angles. Only the *high*-frequency components of the oscillations in bonds and valence angles are removed, and significant changes in valence angle can accompany low-frequency torsional motion and are of particular importance in conformational transitions. This result is in accord with results from flexible geometry (or adiabatic) mapping, which showed that rigid ge-

ometry calculations lead to an artificial restriction of the available conformational-phase space and an overestimation of rotational barriers.[43] However, unlike adiabatic mapping, the filtered structures along a trajectory correspond to average structures due to high-frequency vibrations and not the structures corresponding to the lowest energy. In other words, adiabatic mapping yields idealized "zero temperature" structures whereas the filtered trajectory results in realistic "effective" transient structures. When combined with filtering of the corresponding energy trajectories,[24] this technique can provide unique information about structural and energetic changes during conformational transitions.

(43) Stern, P. S.; Chorev, M.; Goodman, M.; Hagler, A. T. *Biopolymers* **1983**, *22*, 1885-1900.

Registry No. I, 60-35-5; II, 22715-68-0.

The Nature of Doubly Charged $C_3H_4^{2+}$ Ions: Structural and Energetic Relationships

Koop Lammertsma*,† and Paul von Ragué Schleyer*,‡

Contribution from the University of Alabama at Birmingham, Department of Chemistry, UAB Station 219 PHS, Birmingham, Alabama 35294, and the Institut für Organische Chemie der Friedrich-Alexander Universität Erlangen-Nürnberg, D-8520 Erlangen, Federal Republic of Germany. *Received January 16, 1990*

Abstract: The singlet and triplet allene dications prevail on the $C_3H_4^{2+}$ potential hypersurface at higher levels of ab initio theory. The global minimum, the planar allene dication **1**, lies in a deep potential well with a deprotonation barrier of 82 kcal/mol. This dication has similar barriers of ca. 15 kcal/mol for scrambling of both its hydrogens and carbons. The existence of a protonated cyclopropenium ion is unlikely. The triplet propyne dication, the least stable isomer studied, is ca. 14 kcal/mol higher in energy than the perpendicular triplet allene dication and is ca. 54 kcal/mol less stable than the planar singlet global minimum **1**.

This paper is concerned with the $C_3H_4^{2+}$ potential energy surface. The isomers **1-10**, studied at reasonably high levels of ab initio theory, reveal unusual structural features and are related to several problems of interest: the nature of $C_3H_4^{2+}$ ions generated in the gas phase, the preference for anti van't Hoff geometries (e.g., for planar tetracoordinate carbons),[1] and the mechanism of the electrophilic substitution of aromatic cyclopropenium ions.[2]

Organic dications are now common in the gas phase, but only some energetic and structural information is available experimentally.[3] Hence, there is an increasing number of theoretical studies of such species: those dealing with the $C_nH_4^{2+}$ series (n = 1, 2, 4, 5, and 6) are most pertinent to the present work.[4]

Although $C_3H_4^{2+}$ ions have been generated by electron impact,[5] by charge exchange,[6] and by charge stripping,[7] no detailed gas-phase data are available. Franklin and Mogenis[5a] reported the observation of $C_3H_4^{2+}$ by electron impact on allene in 1967; ΔH_f° = 743 kcal/mol was estimated from the appearance potential. This value appears to be much too high (heats of formation nearer 600 kcal/mol are to be expected). Proton ejection from $C_3H_4^{2+}$ was observed to be the most likely decomposition pathway.[5a] From the 3.24 Å intercharge distance for this process, calculated from the 4.44 eV kinetic energy released in the charge separation experiment, March suggested $C_3H_4^{2+}$ to have a cyclic structure.[7c] In the present study we show this proposal to be very unlikely. As has been recognized in the literature,[4,8] doubly ionized allene should have a planar singlet ground state **1**; the D_{2d} form **2** as well as the propyne dication **3** should be triplets.

The cyclopropenium ion has twice the resonance energy of benzene.[9] The traditional chemical reaction characteristic of aromatic molecules is their ability to undergo electrophilic substitution, rather than addition. Indeed, H^+/D^+ exchange has been reported experimentally for a cyclopropenium ion with stabilizing substituents.[10] Stimulated by this result, Clark and Weiss[11] investigated such electrophilic substitution reactions of cyclopropenium ions calculationally. Geometries were optimized with the minimal STO-3G basis set, and the final energies were obtained at the split valence 4-31G ab initio level. Several intriguing results for the parent $C_3H_4^{2+}$ species were reported. Among the cyclic isomers (**7-10**), a form **7** with a planar tetracoordinate carbon was found to have the lowest energy. The edge protonated **8**, second in stability, was considerably better than the corner

† University of Alabama at Birmingham.
‡ Institüt für Organische Chemie der Friedrich-Alexander Universität Erlangen-Nürnberg.

(1) Krogh-Jespersen, K.; Cremer, D.; Poppinger, D.; Pople, J. A.; Schleyer, P. v. R.; Chandrasekhar, J. *J. Am. Chem. Soc.* **1979**, *101*, 4843 and references cited therein.
(2) West, R. *Acc. Chem Res.* **1970**, *3*, 130.
(3) For recent reviews, see: (a) Lammertsma, K.; Schleyer, P. v. R.; Schwarz, H. *Angew. Chem., Int. Ed. Engl.* **1989**, *28*, 1321. (b) Koch, W.; Maquin, F.; Stahl, D.; Schwarz, H. *Chimia* **1985**, *39*, 376. (c) Ast, T. *Adv. Mass Spectrom.* **1980**, *8A*, 555. (d) Ast, T. *Adv. Mass Spectrom.* **1986**, *10*, 471. (e) Koch, W.; Schwarz, H. In *Structure/Reactivity and Thermochemistry of Ions*; P. Ausloos, S. G. Lias, Ed.; Reidel Publishing Co.: Dordrecht, 1987; p 413. For reviews on dication in solution, see: (f) Prakash, G. K. S.; Rawdah, T. N.; Olah, G. A. *Angew. Chem., Int. Ed. Engl.* **1983**, *2*, 356. (g) Pagni, R. M. *Tetrahedron* **1984**, *40*, 4161.
(4) (a) Lammertsma, K. *Rev. Org. Intermed.* **1988**, *9*, 141. (b) Schleyer, P. v. R. *Am. Chem. Soc. Div. Pet. Chem. Prepr.* **1983**, *28*, 413.
(5) (a) Franklin, J. L.; Mogenis, A. *J. Chem. Phys.* **1967**, *71*, 2820. (b) Peers, A. M.; Vigny, P. *J. Chem. Phys.* **1968**, *65*, 805.
(6) (a) Brehm, B.; de Frênes, G. *Adv. Mass Spectrom.* **1980**, *8A*, 138. (b) Brehm, B.; Fröbe, U.; Neitzke, H.-P. *Int. J. Mass Spectrom.* **1984**, *57*, 91. (c) Jones, B. E.; Abbey, L. E.; Chatham, H. L.; Honner, A. W.; Telehefsky, L. A.; Burgess, E. M.; Moran, T. F. *Org. Mass Spectrom.* **1982**, *17*, 10.
(7) (a) Rabrenovič, M.; Proctor, C. J.; Ast, T.; Herbert, C. G.; Brenton, A. G.; Beynon, J. H. *J. Phys. Chem.* **1983**, *87*, 3305. (b) Rabrenovič, M.; Herbert, C. G.; Proctor, C. J.; Beynon, J. H. *Int. Mass Spectrom. Ion Phys.* **1983**, *11*, 125. (c) March, R. E. *Org. Mass Spectrom.* **1987**, *22*, 545. (d) Mommers, A. A.; Burgers, P. C.; Holmes, J. L.; Terlouw, J. K. *Org. Mass Spectrom.* **1984**, *19*, 7.
(8) (a) Hoffmann, R. *Tetrahedron* **1966**, *22*, 521. (b) Cuthbertson, A. F.; Glidewell, C. *J. Mol. Struct.* **1982**, *87*, 71.
(9) (a) Krogh-Jespersen, K.; Cremer, D.; Dill, J. D.; Pople, J. A.; Schleyer, P. v. R. *J. Am. Chem. Soc.* **1981**, *103*, 2589. (b) Radom, L.; Hariharan, P. C.; Pople, J. A.; Schleyer, P. v. R. *J. Am. Chem. Soc.* **1976**, *98*, 10.
(10) Weiss, R.; Priesner, C. *Angew. Chem., Int. Ed. Engl.* **1978**, *17*, 445.
(11) Clark, T.; Weiss, R. *J. Org. Chem.* **1980**, *45*, 1790.

0002-7863/90/1512-7935$02.50/0